

UDC 544.643.076.2+544.463

New Nanostructured Vanadium-Containing Cathode Materials for Lithium-Ion Rechargeable Batteries: Mechanochemical Synthesis and Properties

N. V. KOSOVA and E. T. DEVYATKINA

*Institute of Solid State Chemistry and Mechanochemistry, Siberian Branch, Russian Academy of Sciences, Ul. Kutateladze 18, Novosibirsk 630128 (Russia)**E-mail: kosova@solid.nsc.ru*

Abstract

By the mechanochemically stimulated solid-phase synthesis, new nanostructured cathode materials based on vanadium were obtained: $\text{Li}_3\text{V}_2(\text{PO}_4)_3$, LiVPO_4F and their composites $\text{LiVPO}_4\text{F}/\text{Li}_3\text{V}_2(\text{PO}_4)_3$. The crystal structure and electrochemical properties of the synthesized compounds were studied by means of XPA with refinement according to Rietveld and chronopotentiometry. It was demonstrated that $\text{Li}_3\text{V}_2(\text{PO}_4)_3$ is stably cycling within the voltage range 3.0–4.3 V, in particular at high current density. Improvement of the cathode characteristics of LiVPO_4F is promoted by obtaining composite materials $\text{LiVPO}_4\text{F}/\text{Li}_3\text{V}_2(\text{PO}_4)_3$ with nanodomain structure. The possibility to use LiVPO_4F in symmetric cells with the voltage of 2.4 V is demonstrated.

Key words: lithium-ion rechargeable batteries, cathode materials, $\text{Li}_3\text{V}_2(\text{PO}_4)_3$, LiVPO_4F , mechanical activation, crystal structure, cycling

INTRODUCTION

It is known that electrochemical properties of electrode materials for lithium-ion rechargeable batteries are strongly dependent on particle size and morphology. We demonstrated the possibility to obtain a number of nanostructured cathode and anode materials with the help of mechanical activation, and studied the features of their structure and electrochemical properties [1].

During the recent years, much attention is paid to electrode materials based on vanadium. This is connected with the fact that vanadium has several oxidation degrees, so several electrons per the formula unit of the compound may participate in cycling processes. As a result, their specific capacity increases. Among vanadium-based cathode materials under study, specially emphasized compounds are $\text{Li}_3\text{V}_2(\text{PO}_4)_3$ with monoclinic structure (sp. gr. $P2_1/n$) [2–4] and LiVPO_4F with triclinic structure (sp. gr. $P\bar{1}$) [5–14]. The electrochemical ac-

tivity of these compounds is connected with the reversibility of oxidation-reduction pairs $\text{V}^{3+}/\text{V}^{4+}$ and $\text{V}^{4+}/\text{V}^{5+}$.

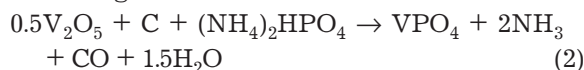
The goal of the present work was to obtain the indicated compounds and their composites in nanostructured state by means of mechanochemically stimulated solid-phase synthesis and to study their structure, morphology and electrochemical properties.

EXPERIMENTAL

The following reagents were used in the synthesis of $\text{Li}_3\text{V}_2(\text{PO}_4)_3$: Li_2CO_3 , V_2O_5 , $(\text{NH}_4)_2\text{HPO}_4$, LiF of Ch. D. A. (pure for analysis) reagent grade, carbon of P 277 KhIT grade manufactured by Institute of Hydrocarbons Processing (IHP) of the SB RAS (Omsk).

The synthesis of $\text{Li}_3\text{V}_2(\text{PO}_4)_3$ was carried out using the carbothermal method according to reaction $3\text{Li}_2\text{CO}_3 + 2\text{V}_2\text{O}_5 + 2\text{C} + 6(\text{NH}_4)_2\text{HPO}_4 \rightarrow 2\text{Li}_3\text{V}_2(\text{PO}_4)_3 + 12\text{NH}_3 + 4\text{CO} + 3\text{CO}_2 + 18\text{H}_2\text{O}$ (1)

The synthesis of LiVO_4F was carried out stepwise: VPO_4 was obtained preliminarily, and then its interaction with LiF was carried out according to reaction



To accelerate the synthesis and obtain the compounds in the nanometer-sized state, the mixtures of reagents were activated preliminarily using AGO-2 mechanical activator (900 min^{-1}). Annealing of activated mixtures was carried out in a tubular furnace in argon flow at a temperature of $700\text{--}800^\circ\text{C}$. Carbon taken as a reducing agent also prevents agglomeration of product particles during subsequent annealing, and its excess may be used to make a surface electron-conducting coating.

The obtained samples were analyzed by means of X-ray phase analysis (XPA) with a D8 Advance Bruker diffractometer (CuK_α radiation, step $0.02^\circ/\text{s}$), scanning electron microscope MIRA3 TESCAN, and by means of galvanic cycling in semi-cells with lithium anode and electrolyte based on 1 M LiPF_6 solution in a mixture of ethylene- and dimethyl carbonate. The lattice parameters were refined by means of Rietveld using GSAS software package.

RESULTS AND DISCUSSION

Lithium vanadophosphate $\text{Li}_3\text{V}_2(\text{PO}_4)_3$

Lithium vanadophosphate $\text{Li}_3\text{V}_2(\text{PO}_4)_3$ with monoclinic structure (sp. gr. $P2_1/n$) belongs to the class of Nasicon-like compounds possessing high ionic conduction [2]. Within the voltage region $3.0\text{--}4.3 \text{ V}$, $\text{Li}_3\text{V}_2(\text{PO}_4)_3$ is able to extract reversibly two Li ions per the formula unit due to the oxidation-reduction pair $\text{V}^{3+}/\text{V}^{4+}$. At the charge up to 4.8 V , the third Li ion may be extracted with the participation of $\text{V}^{4+}/\text{V}^{5+}$ pair, however, this process is hindered kinetically. Depending on the upper voltage of cycling (4.3 and 4.8 V), the theoretical capacity of $\text{Li}_3\text{V}_2(\text{PO}_4)_3$ is 132 and $198 \text{ mA} \cdot \text{h/g}$, and average voltage is 3.8 and 4.0 V , respectively. The charge-discharge curves contain four plateaus corresponding to the sequence of $\text{Li}_3\text{V}_2(\text{PO}_4)_3$ transformations into the final phase $\text{V}_2(\text{PO}_4)_3$.

The diffraction patterns of the obtained $\text{Li}_3\text{V}_2(\text{PO}_4)_3$ sample with refinement using Rietveld method are shown in Fig. 1. One can see that the sample is practically single-phase and is crystallized in the monoclinic symmetry (space group $P2_1/n$). Refined lattice parameters are: $a = 8.6105(4) \text{ \AA}$, $b = 8.6124(3) \text{ \AA}$, $c = 12.0405(5) \text{ \AA}$, $\beta = 90.500(2)^\circ$, cell volume $V = 892.86(8) \text{ \AA}^3$

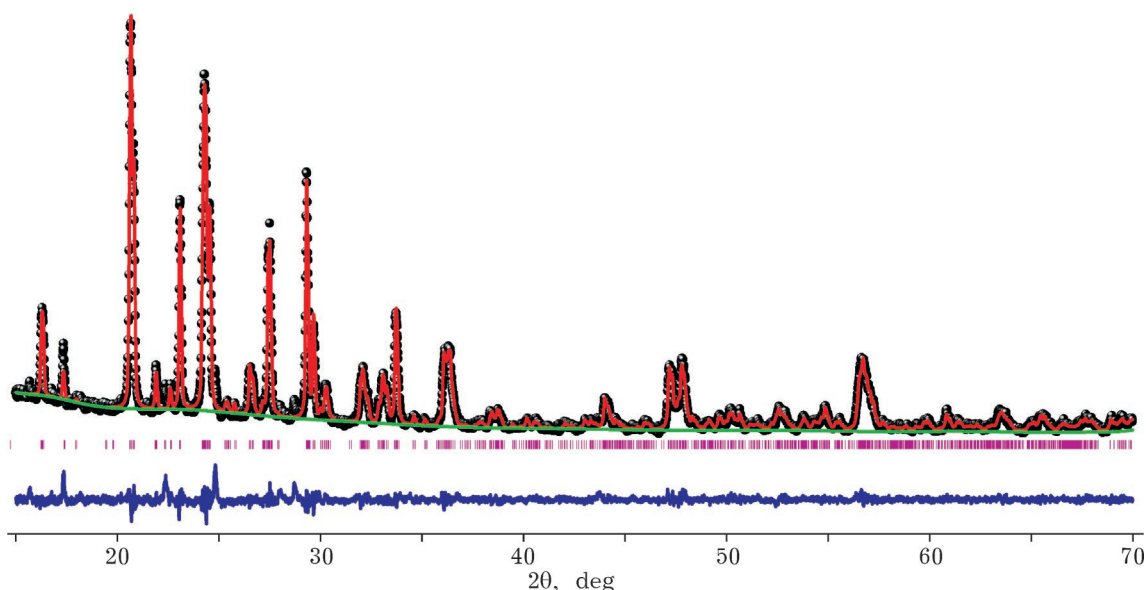


Fig. 1. Diffraction patterns of $\text{Li}_3\text{V}_2(\text{PO}_4)_3$, with refinement according to Rietveld method.

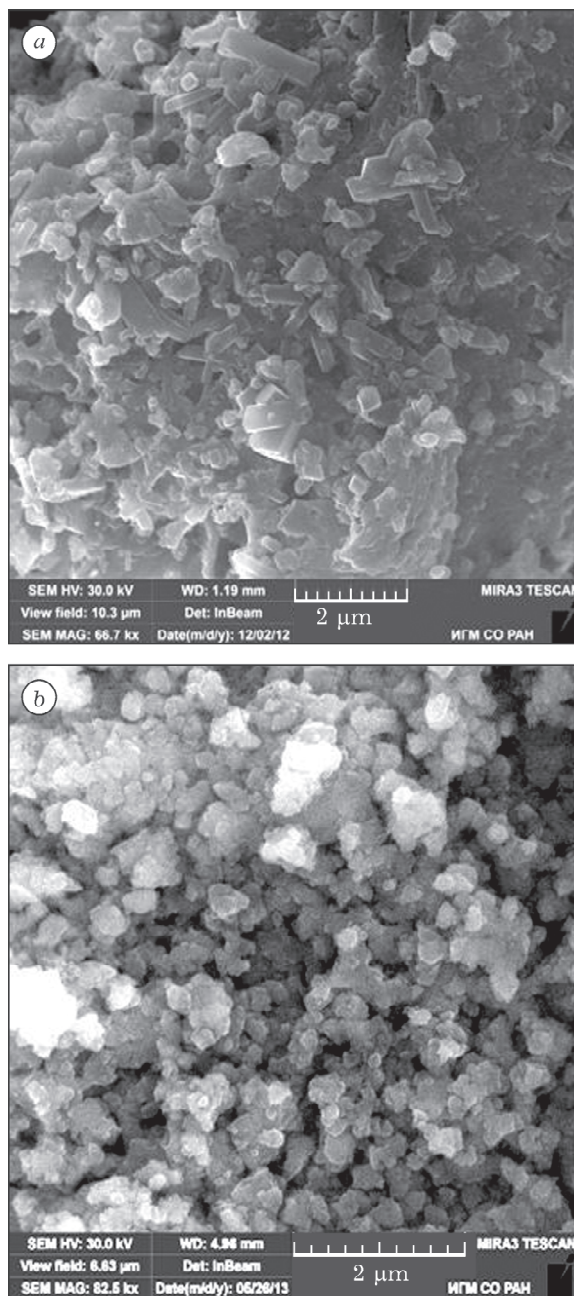


Fig. 2. SEM microphotographs of $\text{Li}_3\text{V}_2(\text{PO}_4)_3$ (a) and LiVPO_4F (b).

($R_{\text{wp}} = 7.99\%$, $R_p = 5.63\%$, $\chi^2 = 2.424$), which is in good agreement with the literature data [3]. In the structure of $\text{Li}_3\text{V}_2(\text{PO}_4)_3$, vanadium atoms are distributed in two independent positions, while lithium ions are distributed in three positions. Two lithium ions have five-coordinated position, and one lithium ion has a four-coordinated position. According to the literature data, lithium diffusion proceeds along the 001 direction.

One can see in the SEM micrograph that the obtained $\text{Li}_3\text{V}_2(\text{PO}_4)_3$ sample is mainly characterized by the particles of prismatic shape with the average longitudinal and cross size 800 and 100 nm, respectively (Fig. 2, a).

The electrochemical properties of $\text{Li}_3\text{V}_2(\text{PO}_4)_3$ were studied by means of galvanostatic cycling within two voltage ranges: 2.5–4.3 and 2.5–4.8 V. The profiles of charge-discharge curves and the dependences $dQ/dE = f(E)$ are presented in Fig. 3. One can see that three plateaus at 3.61, 3.69 and 4.08 V are observed on the charge curves for charging to 4.3 V, and an additional plateau at 4.52 V for charging to 4.8 V, which corresponds to the sequence of phase transformations: $\text{Li}_3\text{V}_2(\text{PO}_4)_3 \rightarrow \text{Li}_{2.5}\text{V}_2(\text{PO}_4)_3 \rightarrow \text{Li}_2\text{V}_2(\text{PO}_4)_3 \rightarrow \text{Li}_1\text{V}_2(\text{PO}_4)_3 \rightarrow \text{V}_2(\text{PO}_4)_3$ [2]. Extraction of the third lithium ion, corresponding to the oxidation-reduction pair $\text{V}^{4+}/\text{V}^{5+}$, is hindered kinetically as a consequence of the low electron-ion conduction of the final phase $\text{V}_2(\text{PO}_4)_3$ [4]. During discharge from 4.3 V, three reduction peaks are present, corresponding to the oxidation-related ones. The close positions

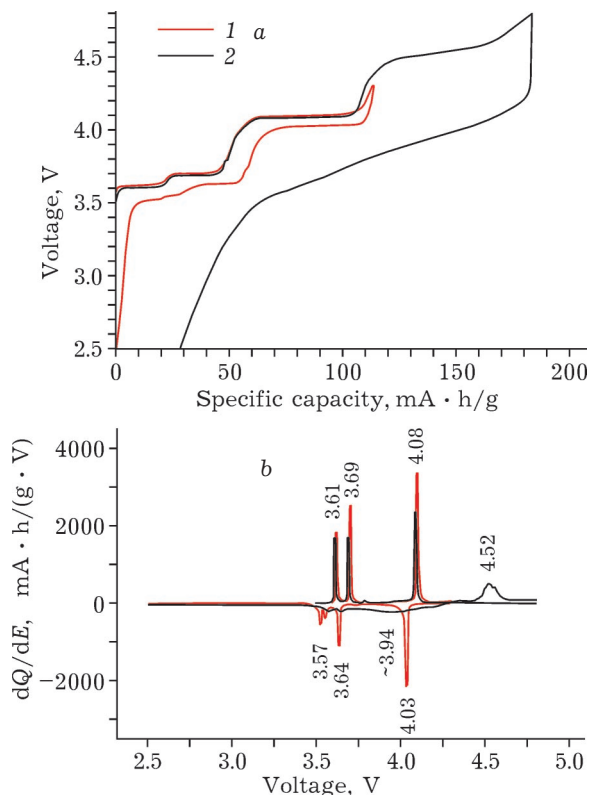


Fig. 3. Charge-discharge profiles of $\text{Li}_3\text{V}_2(\text{PO}_4)_3$ up to the voltage of 4.3 and 4.8 V (a) and dependences $dQ/dE = f(E)$ (b): 1, 2 – during discharging to 4.3 and 4.8 V, respectively.

of oxidation-reduction peaks on the dependence $dQ/dE = f(E)$ points to low polarization degree and non-hindered electron-ion transport. Quite contrary, during discharge from 4.8 V, a sloping profile of the discharge curve is observed within the range $0 < x_{\text{Li}} < 2$ instead of a plateau. As a rule, the sloping profile points to the mechanism of solid solutions (a single-phase mechanism of lithium intercalation). However, after insertion of two lithium ions, a plateau characteristic of the two-phase mechanism appears. Typical plateaus are again observed on subsequent charge curves. Though an increase in the upper voltage limit to 4.8 V leads at first to an increase in the specific discharge capacity of $\text{Li}_3\text{V}_2(\text{PO}_4)_3$, later on we observe its rapid degradation (Fig. 4). The problem is likely to be due to the side interaction of the cathode material with the electrolyte (vanadium dissolution) at high voltage.

The dependence of the specific discharge capacity of $\text{Li}_3\text{V}_2(\text{PO}_4)_3$ on cycling rate C (in mA/g) is shown in Fig. 5. One can see that with an increase in the rate by a factor of 50 (from 0.1C to 5C) the capacity changes only slightly, while with an increase by a factor of 200 (to 20C) it decreases only by one half, which is connected with the high electron-ion conduction of the cathode composite material $\text{Li}_3\text{V}_2(\text{PO}_4)_3/\text{C}$. So, mechanochemically stimulated solid-phase synthesis of $\text{Li}_3\text{V}_2(\text{PO}_4)_3$ involving carbothermal reduction of V_2O_5 allows an easy and simple preparation of the cathode material with good electrochemical properties, not worse than those of the world analogs manufactured us-

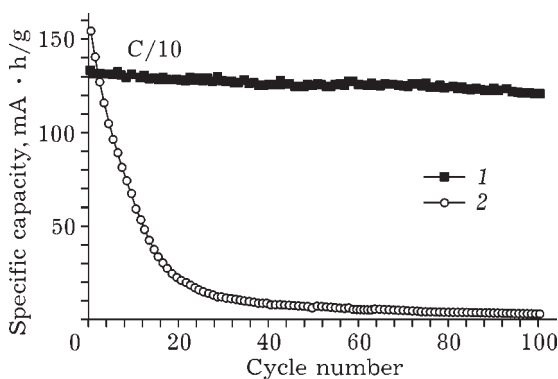


Fig. 4. Dependence of specific discharge capacity of $\text{Li}_3\text{V}_2(\text{PO}_4)_3$ on cycle number during cycling to the voltage of 4.3 V (1) and 4.8 V (2).

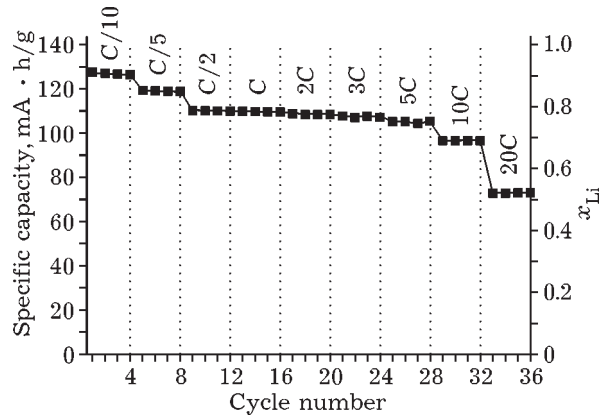


Fig. 5. Dependence of specific discharge capacity of $\text{Li}_3\text{V}_2(\text{PO}_4)_3$ on cycling rate within voltage range 2.5–4.3 V.

ing a more complicated and time-consuming method.

Lithium vanadium fluorophosphate LiVPO_4F

The structural and electrochemical properties of LiVPO_4F were studied for the first time by Barker *et al.* [5]. Lithium vanadium fluorophosphate LiVPO_4F is isostructural to tavorite $\text{LiFePO}_4 \cdot \text{OH}$ and crystallizes in triclinic symmetry (sp. gr. $P1$). Diffusion of lithium ions proceeds along unidimensional channels along the 111 direction [6]. Electrochemical activity of LiVPO_4F is connected with the oxidation-reduction pair $\text{V}^{3+}/\text{V}^{4+}$; the theoretical capacity is 156 mA · h/g. Lithium extraction from LiVPO_4F is described by two two-phase plateaus on charge-discharge curves at 4.24 and 4.28 V with respect to Li. Quite contrary, lithium intercalation is characterized by one plateau at 4.2 V. The working voltage of LiVPO_4F is higher by 0.2 than that of LiCoO_2 and higher by 0.7 V than that of LiFePO_4 . The energy density of LiVPO_4F exceeds the energy density of LiFePO_4 , while the thermal stability of LiVPO_4F is higher than the thermal stability of all the known oxide cathode materials, such as LiMn_2O_4 , LiCoO_2 and LiNiO_2 [7, 8]. The promising properties of fluorophosphates are directly connected with their crystal structure which remains stable during cycling. The volume ionic conduction of LiVPO_4F is approximately $8 \cdot 10^{-7}$, while its electronic conduction is only 10^{-11} S/cm [9].

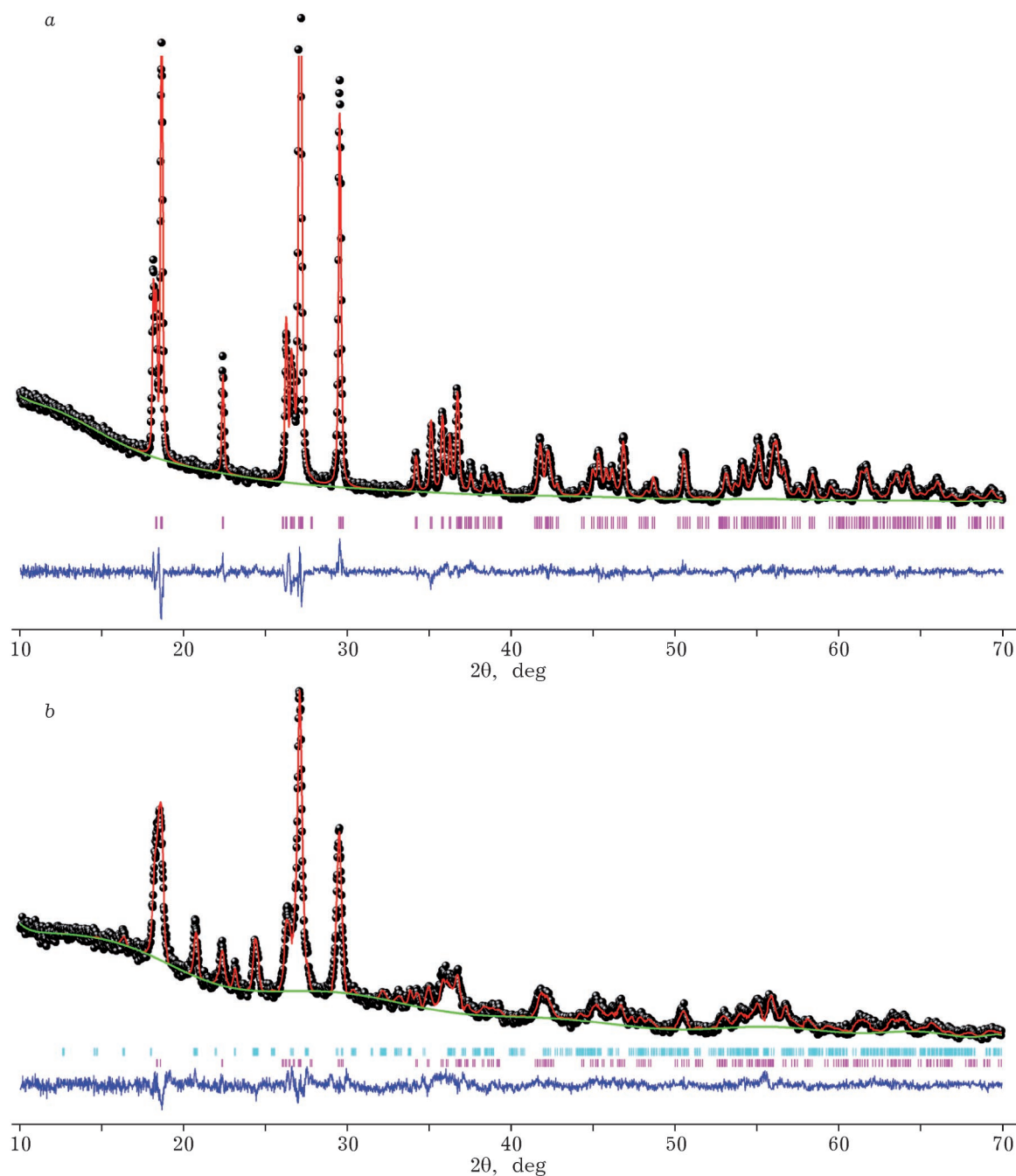


Fig. 6. Diffraction patterns of single-phase LiVPO_4F (a) and composite $\text{LiVPO}_4\text{F}/\text{Li}_3\text{V}_2(\text{PO}_4)_3$ (b) with refinement according to Rietveld method.

In the studies of the synthesis of LiVPO_4F , it was established by us that with an increase in annealing time or temperature, partial decomposition of nanometer-sized occurs, with the evolution of VF_3 into the gas phase, and the formation of the admixture phase $\text{Li}_3\text{V}_2(\text{PO}_4)_3$ according to reaction

$$3\text{LiVPO}_4\text{F} \rightarrow \text{VF}_3 + \text{Li}_3\text{V}_2(\text{PO}_4)_3 \quad (3)$$

The diffraction patterns of the single-phase product LiVPO_4F and the composite $\text{LiVPO}_4\text{F}/\text{Li}_3\text{V}_2(\text{PO}_4)_3$ with refinement according to Rietveld method are shown in Fig. 6. The profile of LiVPO_4F is well described by the triclinic structure with sp. gr. $P\bar{1}$ as the refining model [10]. The compound LiVPO_4F has a three-dimensional framework structure composed of

PO_4 tetrahedrons and VO_4F_2 octahedrons; oxygen ions are common for PO_4 and VO_4P_2 . In this structure, there are two crystallographic positions in which lithium ions are distributed statistically. Vanadium atoms also occupy two different positions and have four oxygen ions and two fluoride ions in their surroundings. Fluorine atoms are located in the vertices of VO_4F_2 octahedrons [6]. The refined parameters of LiVPO_4F lattice are: $a = 5.299(2) \text{ \AA}$, $b = 7.240(2) \text{ \AA}$, $c = 5.163(1) \text{ \AA}$, $\alpha = 107.890(3)^\circ$, $\beta = 98.482(3)^\circ$, $\gamma = 107.529(3)^\circ$, lattice volume $V = 173.3(1) \text{ \AA}^3$ ($R_{\text{wp}} = 5.91 \%$, $R_p = 4.59 \%$, $\chi^2 = 1.712$).

The diffraction patterns of the composite $\text{LiVPO}_4\text{F}/\text{Li}_3\text{V}_2(\text{PO}_4)_3$ contain two sets of reflections relating to the triclinic phase LiVPO_4F with sp. gr. $P1$ and to the monoclinic phase $\text{Li}_3\text{V}_2(\text{PO}_4)_3$ with sp. gr. $P2/n$. The refined parameters of the lattice of the major phase LiVPO_4F are somewhat different from the parameters of the previous sample: $a = 5.296(1) \text{ \AA}$, $b = 7.250(1) \text{ \AA}$, $c = 5.193(1) \text{ \AA}$, $\alpha = 107.72(2)^\circ$, $\beta = 98.63(1)^\circ$, $\gamma = 107.49(1)^\circ$, lattice volume $V = 174.63(7) \text{ \AA}^3$ ($R_{\text{wp}} = 5.67 \%$, $R_p = 4.36 \%$, $\chi^2 = 1.822$). The lattice parameters

of the admixture phase $\text{Li}_3\text{V}_2(\text{PO}_4)_3$ are close to the data reported in [4]: $a = 8.603(3) \text{ \AA}$, $b = 8.589(3) \text{ \AA}$, $c = 12.037(4) \text{ \AA}$, $\beta = 90.27(6)^\circ$, lattice volume $V = 889.4(5) \text{ \AA}^3$. The mass ratio $\text{LiVPO}_4\text{F}/\text{Li}_3\text{V}_2(\text{PO}_4)_3$, determined by means of multiprofile refinement, is 85 : 15.

According to SEM data, the obtained samples are nanostructured (see Fig. 2, b). The average particle size is approximately 100 nm.

The synthesized LiVPO_4F and $\text{LiVPO}_4\text{F}/\text{Li}_3\text{V}_2(\text{PO}_4)_3$ samples were cycled in two voltage ranges: 3.0–4.5 and 1.3–2.5 V (Fig. 7). One can see that the charge curve of LiVPO_4F in the first voltage range has a two-step profile, while the discharge curve has a single plateau, which is typical for LiVPO_4F . The inflection of the charge curve is observed at $x_{\text{Li}} \sim 0.338$ and corresponds to the formation of the intermediate phase $\text{Li}_{0.67}\text{VPO}_4\text{F}$ [11, 12]. The final phase of lithium deintercalation from LiVPO_4F is VPO_4F with sp. gr. $C2/c$; the process is accompanied by the compression of the unit cell by approximately 8 % in comparison with LiVPO_4F [13]. Insertion of Li into the lattice of VPO_4F during discharge proceeds according to a different

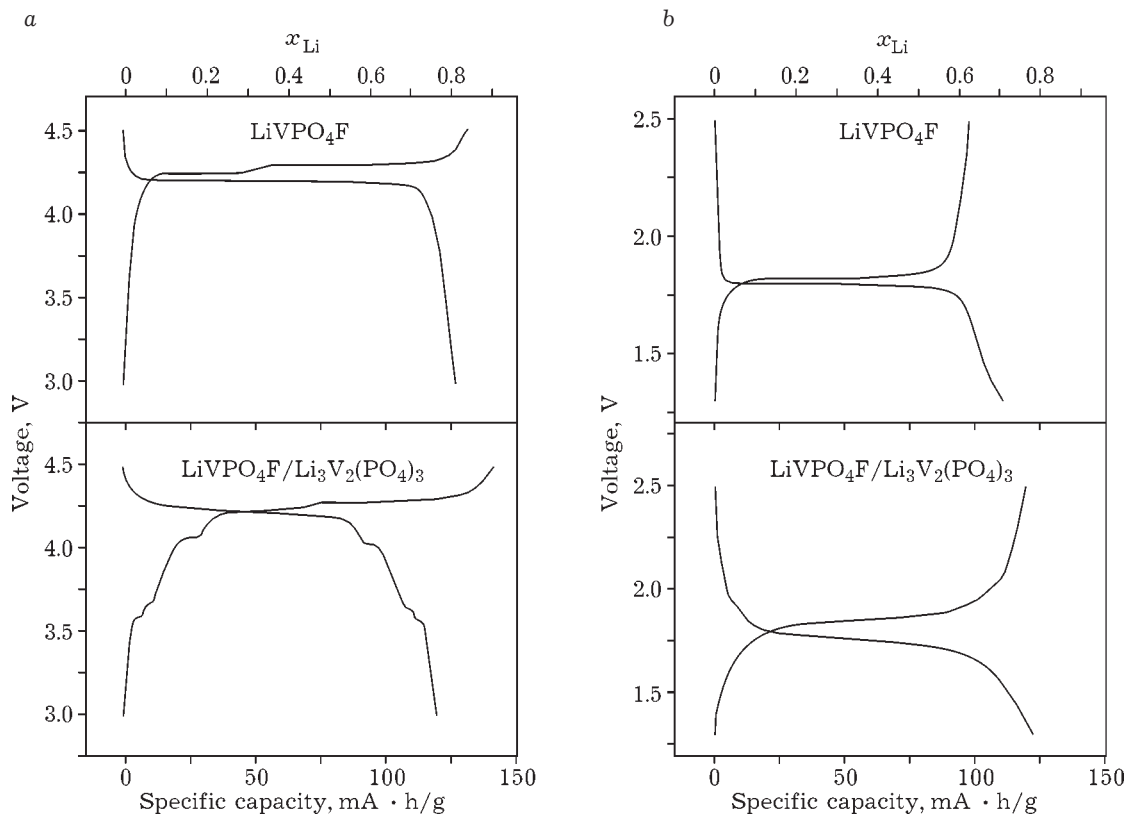


Fig. 7. Charge-discharge profiles of LiVPO_4F within voltage range 3.0–4.5 (a) and 1.3–2.5 V (b).

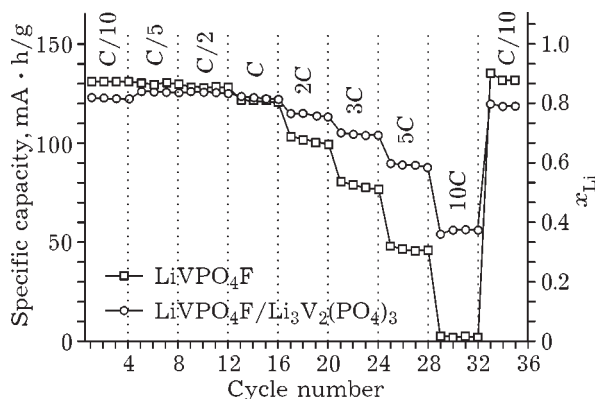


Fig. 8. Dependence of specific discharge capacity of LiVPO_4F and composite $\text{LiVPO}_4\text{F}/\text{Li}_3\text{V}_2(\text{PO}_4)_3$ on rate within voltage range 3.0–4.5 V.

mechanism than that of Li extraction from LiVPO_4F . Though the mechanism remains two-phase (a plateau is observed on the discharge curve), the intermediate phase $\text{Li}_{0.67}\text{VPO}_4\text{F}$ is not formed. The charge-discharge profile of the composite $\text{LiVPO}_4\text{F}/\text{Li}_3\text{V}_2(\text{PO}_4)_3$ has a more complicated shape: during charging in the voltage range of 4.1–4.5 V, it is characterized by two-step process, typical for LiVPO_4F ; however, during discharge, instead of a single-stage plateau we observe a sloping curve. This may be a consequence of the change of two-phase mechanism of lithium intercalation to the single-phase one (the mechanism of solid solutions). In the region of 3.0–4.3 V, additional steps appear on charge-discharge curves at 3.56, 3.64 and 4.04 V, corresponding to the admixture phase $\text{Li}_3\text{V}_2(\text{PO}_4)_3$.

The specific discharge capacity of LiVPO_4F and $\text{LiVPO}_4\text{F}/\text{Li}_3\text{V}_2(\text{PO}_4)_3$ samples within voltage range 3.0–4.5 V is 132 and 125 mA·h/g, respectively. Low polarization is observed, which is due to rapid ion transport. It follows from the data shown in Fig. 8 that LiVPO_4F and $\text{LiVPO}_4\text{F}/\text{Li}_3\text{V}_2(\text{PO}_4)_3$ are also well cycled at the high rates of charging-discharging, which is their advantage in comparison with other polyanionic cathode materials (LiMPO_4 , where $M = \text{Fe}, \text{Mn}$). At high cycling rates, the properties of the composite exceed those of single-phase LiVPO_4F . This may be connected with the nanodomain structure of the composite and the presence of superionic conductor $\text{Li}_3\text{V}_2(\text{PO}_4)_3$. The amount of electrochemically active component $\text{Li}_3\text{V}_2(\text{PO}_4)_3$ in the composite, determined from the electrochemical data, reaches 10 mol. %, which is in good agreement with the XPA data.

Recently, the possibility to insert additional Li into the structure of LiVPO_4F in the region of lower voltage (1.8 V) was demonstrated, which is connected with the oxidation-reduction pair $\text{V}^{3+}/\text{V}^{2+}$; the theoretical capacity is 156 mA·h/g [14]. It was established by means of *in situ* XPA that the insertion of additional Li into LiVPO_4F occurs according to the two-phase mechanism [12]. The final phase is $\text{Li}_2\text{VPO}_4\text{F}$ crystallized in the sp. gr. C2/c [13].

The charge-discharge curves of LiVPO_4F and $\text{LiVPO}_4\text{F}/\text{Li}_3\text{V}_2(\text{PO}_4)_3$ within voltage range 1.3–2.5 V are shown in Fig. 7, b. It is interesting that at the voltage of ~1.8 V the single-phase sample is characterized by the presence of a

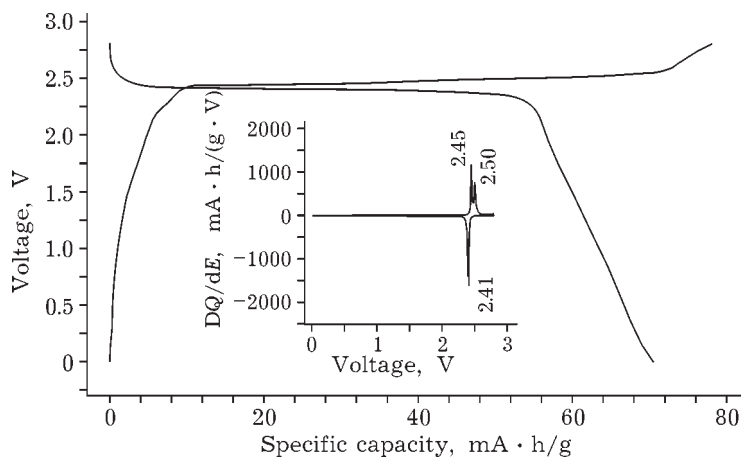


Fig. 9. Charge-discharge curves of the symmetrical cell $\text{LiVPO}_4\text{F}/\text{LiVPO}_4\text{F}$. Dependence $dQ/dE = f(E)$ is shown in the insert.

plateau on the curve, while the composite $\text{LiVPO}_4\text{F}/\text{Li}_3\text{V}_2(\text{PO}_4)_3$ is characterized by the sloping curve. So, the samples demonstrate the same differences as those observed during sample cycling within the high voltage region.

Relying on the possibility of cycling LiVPO_4F within two voltage ranges, we studied the electrochemical behaviour of the symmetrical cell in which LiVPO_4F serves as cathode and as anode. The obtained charge-discharge curves (Fig. 9) exhibit a plateau at the voltage of 2.4 V; specific discharge capacity is 70 mA · h/g.

CONCLUSION

It is demonstrated that the new promising nanostructured cathode materials based on vanadium – $\text{Li}_3\text{V}_2(\text{PO}_4)_3$ and LiVPO_4F – can be successfully obtained using mechanochemically stimulated solid-phase method. The synthesized $\text{Li}_3\text{V}_2(\text{PO}_4)_3$ is stable when cycled within the voltage range 3.0–4.3 V, in particular, in the case of the high current density. Improvement of the cathode characteristics of LiVPO_4F can be achieved by obtaining composite materials $\text{LiVPO}_4\text{F}/\text{Li}_3\text{V}_2(\text{PO}_4)_3$ with nanodomain structure. The pos-

sibility to use LiVPO_4F in symmetrical cells with the working voltage of 2.4 V was demonstrated.

REFERENCES

- 1 Kosova N. V., Devyatkina E. T., *Electrokhim.*, 48, 2 (2012) 351.
- 2 Huang H., Yin S. C., Kerr T., Taylor N., Nazar L. F., *Adv. Mater.*, 14, 21 (2002) 1525.
- 3 Patoux S., Wurm C., Morcrette M., Rousse G., Masquelier C., *J. Power Sources*, 119–121 (2003) 278.
- 4 Saidi M. Y., Barker J., Huang H., Swoyer J. L., Adamson G., *J. Power Sources*, 119–121 (2003) 266.
- 5 Barker J., Saidi M. Y., Swoyer J. L., *J. Electrochem. Soc.*, 150 (2003) A1394.
- 6 Mueller T., Hauter G., Jain A., Ceder G., *Chem. Mater.*, 23 (2011) 3854.
- 7 Gover R. K. B., Burns P., Bryan A., Saidi M. Y., Swoyer J. L., Barker J., *Solid State Ionics*, 177 (2006) 2635.
- 8 Zhou F., Zhao X., Dahn J. R., *Electrochem. Commun.*, 11 (2009) 589.
- 9 Xiao P. F., Lai M. O., Lu L., *Solid State Ionics*, 242 (2013) 10.
- 10 Ramesh T. N., Lee K. T., Ellis B. L., Nazar L. F., *Electrochem. Solid-State Lett.*, 13 (2010) A43.
- 11 Ateba Mba J. M., Masquelier C., Suard E., Croguennec L., *Chem. Mater.*, 24 (2012) 1223.
- 12 Ateba Mba J. M., Croguennec L., Basier N. I., Barker J., Masquelier C., *J. Electrochem. Soc.*, 159 (2012) A1171.
- 13 Ellis B. L., Ramesh T. N., Davis L. J. M., Govard G. R., Nazar L. F., *Chem. Mater.*, 23 (2011) 5138.
- 14 Barker J., Gover R. K. B., Burns P., Bryan A., *Electrochem. Solid-State Lett.*, 8 (2005) A285.